The Behavior of Antioxidant Irganox 1010 during the Thermal Degradation of a Plastic Bonded Explosive

Yang, Dali
Edgar, Alexander Steven
Rosales, Christopher James
Upshaw, David

To be published in: Polymer Degradation and Stability

DOI to publisher's version: 10.1016/j.polymdegradstab.2022.109928

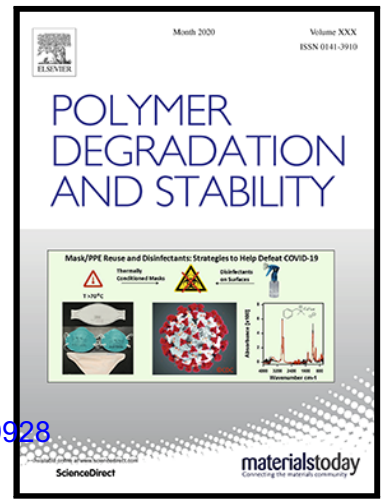

The Behavior of Antioxidant Irganox 1010 during the Thermal Degradation of a Plastic Bonded Explosive

Dali Yang , David A. Upshaw , Alexander S. Edgar , Christopher J. Rosales

PII: S0141-3910(22)00105-7
DOI: https://doi.org/10.1016/j.polymdegradstab.2022.109928
Reference: PDST 109928

To appear in: *Polymer Degradation and Stability*

Received date: 16 December 2021
Revised date: 29 March 2022
Accepted date: 30 March 2022

Please cite this article as: Dali Yang , David A. Upshaw , Alexander S. Edgar , Christopher J. Rosales , The Behavior of Antioxidant Irganox 1010 during the Thermal Degradation of a Plastic Bonded Explosive, *Polymer Degradation and Stability* (2022), doi: https://doi.org/10.1016/j.polymdegradstab.2022.109928

Highlights

- At the early stage, NP tends to degrade more under dry conditions than wet conditions.
- Oxidants, radicals, and acidic molecules generated from NP degradation are predominant species to consume Irg1010 in the PBX 9501 matrix.
- As Irg1010 is completely consumed, oxidation of NP and Estane will take place in PBX 9501, and the molecular weight of Estane will changes non-monotonically over time.

The Behavior of Antioxidant Irganox 1010 during the Thermal Degradation of a Plastic Bonded Explosive

Dali Yang[a,*] dyang@lanl.gov, David A. Upshaw[b,†], Alexander S. Edgar[a], Christopher J. Rosales[c,‡]

[a]MST-7: Engineered Materials, MST Division

[b]Weapon Stockpile Modernization Division

[c]M-7: High Explosive Technology, M Division, Los Alamos National Laboratory, Los Alamos, New Mexico 87545

[*]Corresponding author: Dali Yang

[†]Present address: McMurry University, Department of Physics, 1 McMurry University, Box 38, Abilene, TX 79697

[‡]Present address: Actinide Materials Processing and Power Division, Los Alamos National Laboratory

Abstract

The effect of water concentration on the aging behavior of blend components in plastic bonded explosive (PBX) 9501 is investigated when the samples were aged up to 24 months under various conditions. The blend components studied here are: poly(urethane ester) (Estane®5703) (Estane), nitroplasticizer (NP), and antioxidant Irganox 1010 (Irg1010). The experimental results reveal that NP is prone to thermally degrading and producing H_2O, NO_x and HNO_x species, which are the predominant species to consume Irg1010 during PBX 9501 aging under inert environment. As Irg1010 is completely consumed, Estane degrades through oxidation and NP addition in addition to well anticipated hydrolysis. The competition among hydrolysis, oxidation, and NP addition results in non-monotonical changes in the molecular weight of Estane over the aging process.

Key Words

PBX 9501, Estane®5703, nitroplasticizer, BDNPA/F; Irganox 1010, oxidation, hydrolysis

1. Introduction

Plastic bonded explosive (PBX) 9501 formulation is comprised of, by weight, 94.9% cyclotetramethylene-tetranitramine (HMX), 2.5% poly(urethane ester) (Estane®5703) (called Estane hereinafter), 2.5% nitroplasticizer (NP), and ~0.1 wt% Irganox 1010 (Irg1010) (used as an antioxidant). NP is a eutectic mixture of bis-2,2-dinitropropyl acetal (BDNPA) and bis-2,2-dinitropropyl formal (BDNPF), with an approximate weight ratio of 1:1. It also contains a trace amount of N-phenyl-β-naphthylamine (PBNA) (i.e., ~0.1 wt%) for the purpose of long-term storage, which was added after NP production for scavenging NO_x radicals formed from NP degradation [1].

The combination of Estane and NP forms a polymer binder to coat and bind the HMX particles, provides flexibility to the high explosive (HE) materials, and reduces the sensitivity of HE in machining and handling processes.

Estane is a linear segmented block copolymer (see Figure 1), containing: hard segments - produced from 4,4'-diphenylmethane-diisocyanate (MDI) and 1,4-butanediol, as chain extender; and soft segments - composed of polyester repeat units, produced from adipic acid with 1,4-butanediol. While the soft segments link the hard segments together, they also lend a degree of flexibility and provide mechanical strain (elongation) for the polymer. On the other hand, the hard segments provide mechanical strength (resistance to compression and tensile stress) for the polymer [1-4]. Previous studies have shown that Estane and other constituents of PBX 9501, such as NP and Irg1010, degrade over time, altering material properties [1, 5-8]. Of particular interest is hydrolytic chain scission at the ester group in Estane. This reaction leads to reduced molecular weight and changes in the chemical structure of Estane [2, 6, 9], and thus the mechanical properties of polymer and its composite [5]. However, the aging behavior of Irg1010 is rarely discussed except for the awareness of its depletion, most likely due to scavenging oxidants in the PBX 9501 matrix. Since Irg1010 is an ester based antioxidant, it is subject to hydrolysis as well [10]. The possibility of its hydrolysis is rarely discussed in PBX 9501 applications.

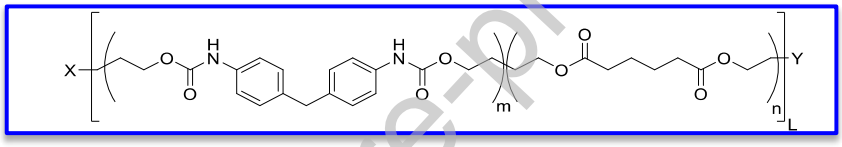

Figure 1. Chemical structure of Estane polymer (m=1-3 and n=4-6). Red background indicates hard segments, blue indicates soft segments.

Early studies have demonstrated that a trace amount of water plays an essential role in altering NP degradation [11, 12]. As illustrated in Figure 2, we hypothesize that NP degradation primarily starts from HONO elimination under moderate temperatures (e.g., 55°C and below) [13-16]. Although the estimated activation energy is as high as 42 kcal/mol in the gas phase [14], the high preexponential factor does not diminish its occurrence [12]. In the condensed phase, the activation energy is as low as 15 kcal/mol while the preexponential factor decreases accordingly, suggesting the degradation of NP exhibits a kinetic compensation effect [12]. A similar phenomenon is observed in the HMX degradation [17]. Nevertheless, HONO decomposition is highly sensitive to temperature, humidity, and headspace conditions [12]. In highly heterogeneous phase, like PBX 9501, micropores inside the HE matrix provide local headspace for vapor to escape, which could promote HONO decomposition. In the presence of adequate water molecules, HONO decomposes into HNO_3 and HNO, and finally into N_2O and H_2O and HNO_3 through Reaction (a) as a net reaction ($4HONO \rightarrow N_2O + H_2O + 2HNO_3$) of a series of reactions ($HONO + HNO_3 \rightarrow 2NO_2^+NO_3^- + H_2O$; $2NO_2^+NO_3^- + 2HONO \rightarrow [HNO]_2 + 4HNO_3$; $[HNO]_2 \rightarrow N_2O + H_2O$). A similar reaction happens between HONO and H_2SO_4 when the H_2SO_4 concentration is very high [18], which is the case in the NP liquid where the water is scarce and acidity is very high. This reaction might be one of reasons why N_2O has been routinely detected in the headspace of aged PBX 9501 containers even at very earliest stages of aging and at 40°C [19]. The presence of water could react with NO_2 to form HNO_3 and slows down HONO decomposition through Reaction (a) in Figure 2. On

the contrary, under dry conditions, HONO molecules decompose into NO_x and water molecules through Reaction (b). These volatile species can diffuse into vapor phase and rapidly attack NP, NP residuals, and polymers through radical oxidation and acid-catalytic hydrolysis. The consumption of NO_x and water through diffusion/reaction shifts HONO elimination forward. Hence, it is expected and observed that NP tends to degrade more and is more sensitive to the headspace of an aging container under dry conditions than under wet conditions at moderate temperatures [13, 14]. Furthermore, HONO and NO_x (radicals) are strong oxidants. Their generation plays a key role in driving the degradation mechanism of Estane away from well anticipated hydrolysis toward oxidation. Hence, humidity plays a key role in changing the properties of NP, Estane, and Irganox. The role of antioxidants is vital for the stabilization of NP and Estane in the PBX 9501 application.

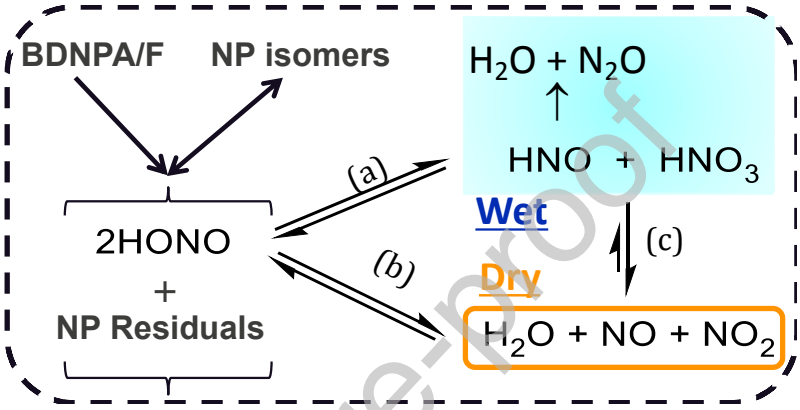

Figure 2. HONO elimination as initial steps in NP degradation under "dry" and "wet" conditions.

While there remain some diverging opinions on the exact mechanistic nature and feasibility of initial HONO formation [20], this is neither the focus of this study nor does our interpretation of overall material degradation here depend on absolute clarity for initial HONO generation. This work rather emphasizes the follow-up chemistries and consequences for the combined materials after the initiating steps involving HONO formation have taken place, and after which HONO can then act as a catalytic impurity to trigger follow-up degradation pathways.

The moisture effect on Estane degradation in its NP binder has been studied previously [6, 8], but this effect on Estane degradation in PBX 9501 has not been studied in such great detail as documented here. Although the addition of HMX in the study matrix complicates the possible source of water and NO_x, the large surface area between HMX crystals and binder affects the water storage and transport in the PBX 9501 matrix, which in turn change the kinetics of how the binder and antioxidant degrade in such a heterogeneous phase, compared to when they are just aged in the binder phase. Therefore, to improve our understanding of the aging behavior of Estane, NP, and Irganox, we conducted a series of aging experiments of the PBX 9501 samples under various humidity conditions at 60°C and 80°C over a period of 24 months. Humidity preconditioning was designed to mimic the range of conditions encountered during the fabrication, storage, handling, and transportation of PBX 9501. We have compared the severity of hydrolytic/oxidative degradation exhibited by the PBX 9501 samples aged at three initial water concentrations over the aging process. The following properties were carefully monitored: 1) sample weight (results, as shown in Figure S1, will be discussed in supplementary materials); 2) Estane molecular weight - using multi-detection Gel Permeation Chromatography (GPC); and 3) the concentrations of NP and Irg1010 - using High Performance

Liquid Chromatography (HPLC). Additionally, the structural changes undergone by Estane, NP, and Irg1010 were analyzed using UV-Vis spectroscopy. The objective of this work is to investigate the effects of the three initial humidity conditions on the aging behavior of NP, Estane, and Irganox. The role of antioxidant in the stabilization of PBX 9501 is discussed more specifically.

It is worth noting that compared to the binder (2.7 mg/g at 50% RH), HMX has a much less water solubility (0.017 mg/g at 50% RH) at ambient conditions [21]. Therefore, it is reasonable to assume that the water loss from PBX 9501 is mostly due to water either trapped inside micropores in the PBX 9501 matrix or water dissolved in the binder materials. Furthermore, as a nitro compound, HMX decomposition will generate NO_x as well. However, the early work suggested that HMX degradation becomes detectable at as high as 150°C, it is therefore reasonable for us to assume the generated NO_x at 80°C and below is mostly due to the degradation of NP [17, 22]. These assumptions are implied in the discussion throughout this paper.

2. EXPERIMENTAL

2.1. Materials

Bulk PBX 9501 molding powder was used to make all the HE samples. More than 100 cylindrical pellets (12.7 mm in diameter x 12.7 mm in length) were pressed at more than 200 MPa. The average volume of the "as pressed" HE pellets was 1.6287 ± 0.0020 cm^3, the average weight was 2.9702 ± 0.0007 g, and thus the average density was 1.8236 ± 0.0022 g/cm^3.

2.2. Test Vessels

Test vessels were built from 316L stainless steel components and were comprised of Swagelok 18 mm cap assemblies and 18 mm diameter x 25.4 mm length tube sections. The nominal internal volume of an assembled test vessels is 4.31 cm^3. Several batches of vessels were cleaned using acetone to remove contaminants introduced by machining and handling processes. Thereafter, the vessels were handled with nitrile gloves and stored in sealed boxes to minimize dust accumulation and fingerprint contamination.

2.3. Aging Sample Preparation and Experiments

Figure 3 details three preconditions for the HE samples discussed in this study. Considering their treatments prior to the aging experiment, they are labelled as VDHE, WHE, and VWHE, standing for: very dry HE, wet HE, and very wet HE, respectively. After the HE pellets were machined and weighed, they were placed in a desiccated box for ~30 days. Next, the HE pellets were baked in a vacuum oven for 24 hours at 60°C and 381 torr absolute pressure to make VDHE. Typically, all HE pellets lost 200-300 ppm of weight. After drying, the VDHE samples were stored in a desiccated dry-box before they were sealed inside the testing vessels. The time between drying and loading into the vessels was up to two months. On average, they gained 45 ppm of weight, and it is assumed the weight gained was due to water uptake.

Some of the above dried pellets underwent further treatment to be conditioned with desired water contents. They were placed in one of two humidity chambers at relative humidity (RH) of ~80% and ~95%. To achieve these humidity conditions, saturated ammonium chloride and sodium sulfite were used, respectively [23]. Due to the low water concentration in the HE samples, weight changes are reported in ppm (mass/mass – as used throughout this paper). To convert weight change (ΔWT in

gram) from gram to ppm, the following equation was used: ΔWT (in gram)/$WT_{avg\text{-}HE}$(in gram)*10^6 (in ppm), where $WT_{avg\text{-}HE}$ (gram) is the averaged weight of the 140 VDHE samples after the vacuum-heated drying treatment. Considering the accuracy of the balance (0.1 mg) and the average weight of the HE samples (2.9702 gram), a weight difference of less than 35 ppm is attributed as analytic error. After humidification, the VWHE samples gained ~389 ppm of water while the WHE samples gained ~275 ppm of water. During sample preparation, the VDHE samples were loaded into the vessels and sealed inside a dry nitrogen box. The WHE and VWHE samples were assembled inside the vessels while continuously flowing nitrogen gas through the vessels for ten seconds and then sealed. One sample was constructed for each configuration at each sample removal from their ovens.

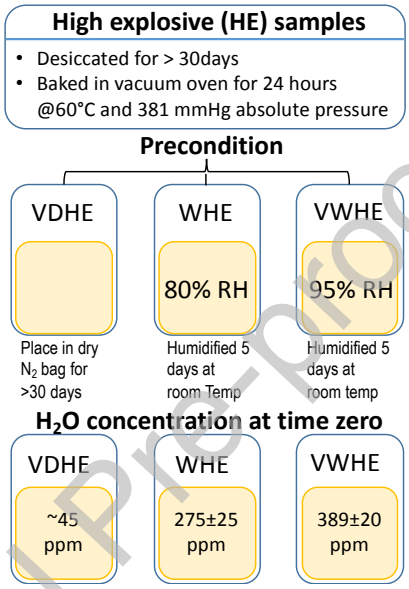

Figure 3. Associated preconditioning procedures and water concentration in the HE samples prior to aging experiments.

Two ovens, one set at 60°C and the other set at 80°C, were used for aging samples. Based on the temperature profiles, the actual aging times are shorter than the anticipated aging time (~93%). The average temperatures of both ovens varied over time, but remained fairly close to 60°C and 80°C on average except for the last 181 days. Due to some down time, the average temperatures were 2–3°C below the target temperatures.

The sample weight was measured upon each removal. Typically, after the vessels were removed from the ovens, they were allowed to cool to room temperature for a few hours before opening. The sample weight was measured immediately after removal from its vessel. After the weight measurement, the samples were sealed in glass vials for photography and sample crushing. More detailed sample handling and preparation are documented in our numerous internal laboratory reports [24].

2.4. Molecular Weight Characterization

2.4.1. GPC Solution Preparation

Prior to GPC solution preparation, the HE samples were crushed into small pieces. Different pieces were selected to create more representative samples for GPC analysis. Duplicate sample solutions were

prepared by dissolving the HE pieces in unstabilized tetrahydrofuran (THF) (Sigma-Aldrich, HPLC grade, >99.9% purity). The target concentration of Estane was 1.5 mg/mL, assuming 2.5 wt% of Estane in the HE samples. The HE pieces were allowed to soak in THF overnight (12–16 hours), and then filtered the next day with a 0.45 μm polytetrafluoroethylene (PTFE) filter. Due to dissolution issues, the samples aged for 4–12 months at 80°C were soaked in THF over an entire weekend (~96 hours) prior to GPC analysis. For most samples, GPC analyses were performed within two to three days after sample removal. The samples were kept in a refrigerator (~6°C) if unable to be analyzed timely. At each interval, instrument verification and control samples were analyzed along with the aged samples. When not in use, these control samples were also stored under refrigeration. Typically, differences between GPC solutions were often observed due to heterogeneity in the HE samples, which became more evident in the longer aged samples.

2.4.2. GPC Analysis

GPC analysis was conducted in two laboratories for cross-checking. One set of analyses was conducted using a conventional GPC, which was only equipped with a differential refractive index (DRI) detector. These results were documented in the internal reports [24]. The other set of GPC analysis was conducted using a multi-detection GPC system, which consisted of a Waters Alliance 2695 separation module, a Wyatt Optilab T-rEX DRI, a Wyatt DWAN Heleos II^{TM} multi-angle light scattering (MALS) detector, a Wyatt ViscoStar$^{®}$ viscometer, and a Waters 996 photodiode array (PDA) detector. Agilent PLgel 5 μm Mixed C and D columns (in series) (7.5 mm i.d. x 300 mm) were used for the samples aged for 0, 4, and 9 months. For direct comparison of the results obtained from the two laboratories, two Agilent PLgel 5 μm Mixed-C columns (in series) (7.5 mm i.d. x 300 mm) were used for the samples aged for 12 months and after. The difference between these two sets of column settings was carefully evaluated and shown to be insignificant [25]. An Agilent PLgel 5 μm guard column was added in front of the GPC columns to protect the columns from potential particles present in the solution and mobile phase. The guard column, GPC columns, and all detectors were held at 40°C, except for the PDA detector, which was operated at room temperature. Polystyrene (PS) narrow standards (Polymer Labs) with known M_p (molecular weight at the GPC peak) at 30 and 200 kDa were used to normalize the MALS detector at different angles. Agilent EasiCal PS2A and 2B standards (580 – ~385 kDa) were used to calibrate the DRI and PDA detectors. These calibration curves were used to calculate the molecular weight and molecular weight distribution based on the retention time of the polymer peak and the peak area. The mobile phase was unstabilized THF at a flow rate of 1.0 mL/min. Since this study lasted more than three years, the batch of THF had changed for different pulls, but was typically the same within each pull. The injection volume was 50 μL for the standards, 75 μL for most aged samples, and 100 μL for severely degraded samples due to low Estane concentration (e.g., 24-month VDHE sample aged at 80°C). Run time was 30 minutes. To determine the concentration of Estane and Irganox, their calibration curves were constructed from pristine Estane and Irg1010 with different concentrations, respectively. In the data analysis, the integration stops at 16.0 min for the PDA detector and 16.5 min for the DRI detector, which is equivalent to the M_p of ~3.5 kDa relative to the PS standard. The GPC data were evaluated using Waters Empower 3 and Wyatt ASTRA 7.3 software, and the UV-vis spectra were retrieved from Waters Empower 3 as well.

2.5. HPLC and Sample Preparation

The aged samples were analyzed by HPLC to determine the Irg1010 concentrations in PBX 9501. A Shimadzu Scientific Instruments Prominence HPLC system equipped with a PDA SPD-M20A detector which was set to collect three dimensional data from 190-400 nm. The PDA was also set to collect data at 230 nm. The system also contains two LC-20AD pumps, a SIL-20AHT auto sampler, and a CTO-20AC column oven set at 40°C. The injection volume was 5 μL into a Waters Symmetry C8 LC column; a 3.5 μm column (4.6 mm i.d. x 100 mm) with a Phenomenex C8 guard column (PN AJ0-4289). Burdick & Jackson HPLC grade methanol/water (M/W) plus 0.010 M ammonium acetate was used as a mobile phase. Isocratic methods were used for the Irg1010 (M/W = 95/05) analysis. The flow rate was 1.2 mL/min. To prepare HPLC solutions, the crushed HE samples were weighed in duplicate. 1 mL of dichloroethane was added to each sample, and the solutions were shaken on a wrist shaker. ~2 mL of HPLC-grade methanol was then added to each vial to make less than 85 mg of HE samples per mL of solvent, and they were shaken again. Upon removing the vials from the wrist shaker, they were centrifuged. After centrifuging, they were filtered with a PTFE syringe filter (0.45 μm). From the filtered sample supernatant, samples were prepared to test Irg1010 concentration. Similar to the GPC analysis, two more samples were prepared for instrument verification and control.

3. Results and Discussion

3.1. Control HE Samples

3.1.1. Molecular Weight

The weight average molecular weight (M_w) of Estane extracted from PBX 9501 sample is 124.8 ± 3.2 kDa from the DRI detector, 123.7 ± 1.5 kDa from the PDA detector, or 71.9 ± 0.3 kDa from the MALS detector at time zero. The M_ws obtained from both DRI and PDA detectors are relative to the PS standards in unstabilized THF. The M_w of Estane from the MALS detector is the absolute M_w. This is about approximate 58% of that obtained from the DRI detector. These results are consistent with the literature reported values [6]. The M_w of the control sample is also monitored over the aging process. The overall change is less than 5% and within the error of the GPC technique (± 5%) [26]. Hence, we conclude that the control sample preserves its properties when stored in the refrigerator.

3.1.2. GPC Elugram and UV Spectrum

Figure 4 (bottom) shows a GPC elugram of a control sample obtained from the PDA detector. The elugram follows a Gaussian distribution. Figure 4 (top) shows the UV spectra obtained for the various fractions at retention times. These UV spectra are identical regardless of their M_ps. The key functional groups in the hard segments in Estane are one diphenylmethane and two urethane groups. Due to the strong extinction coefficient of the diphenyl moiety [27], Estane gives a unique and strong UV peak at ~248 nm with a broad shoulder at ~270 nm and a weak peak at ~282 nm (>C=O).

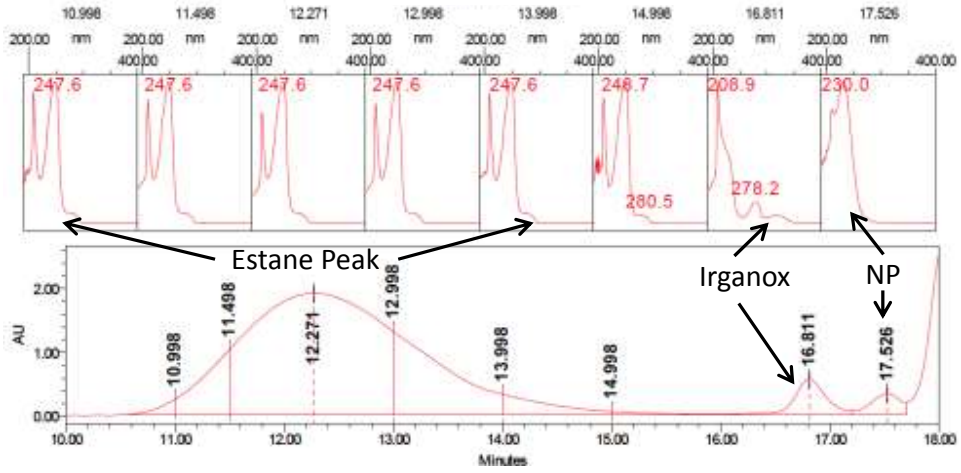

Figure 4. GPC elugram (bottom) and corresponding UV spectra at specific retention times (top) of the control sample. Detailed integration method is given in the GPC section of Supplementary Materials.

In the GPC elugrams, small molecules which had not reacted with Estane, such as Irg1010 and NP, were extracted from the HE samples and chromatographically separated from Estane to give their own peaks and UV spectra. The structure of NP is relatively simple and exhibits one characteristic peak at 231 nm, associated with the C-NO_2 groups. The observed small peak at 210 nm could also be associated with -NO_2 group [28] and/or impurities from solvent and mobile phase.

The UV spectrum of Irg1010 obtained from the control sample exhibits three features: one intense peak at 209 nm and two shoulders at 278 nm and 317 nm. According to a Shimadzu technical note [29], the UV spectrum of Irg1010 should contain two characteristic peaks: 209 and 278 nm, associated with the -COO- in C(-CH_2OO-)$_4$ and >C=O, respectively, when dissolved in THF. The additional peak at 317 nm in the control sample implies some degradation prior to the aging experiment, which may explain why the Irg1010 concentration (<0.068 wt%) is below the anticipated 0.1 wt% at time zero. In an early work conducted by N. Allen [30, 31], the author reported that Irg1010 could be partially or completely oxidized in a catalytic process, degrading to their corresponding quinones by reacting with nitroxyl radicals (NO_x•). The presence of quinones is believed to be responsible for the 317 nm peak, at least in part for the "antagonistic effect" – the ability of the antioxidant to destroy or react with oxidants/radicals. Here, the 317 nm peak might be also associated with the nitroxyl radicals, which are suspected to come from the NP degradation [19, 32, 33]. In summary, Table 1 lists tentative peaks associated with Estane, NP, Irg1010 and degraded products. With this information in mind, one can investigate structural changes occurring during the degradation of Estane, Irganox, and NP aged in the HE samples.

Table 1. Summary of peaks seen in the UV spectra of Estane, aged Estane, NP, and Irganox 1010, tentatively associated functional groups, and possible degradation mechanisms. Ben - benzene ring, SS – soft segments and HS – hard segments, BHT – butylated hydroxytoluene.

Peak position (nm)	Tentatively associated functional group	Associated segments/species	Reaction/cause
200–210	-COOH (carboxylic acid)	Hydrolyzed SS/Estane, Irganox	Hydrolysis
205–210	-COOR(esters)	SS/Estane, Irganox	
210	-NO_2 (nitro) (strong)	NP	NP addition

210, 280-300	-CHO (strong), -CHO (weak)		NP degradation
220-230	-ONO	NP	NP degradation/rearragnement
229	C=C-NO_2	NP	Degradation of NP, NP isomer/residuals
231	C-NO_2	NP	
234, 287	Ben-NH_2 (Aniline)	Urethane in HS	Non-hydrolytic scission
246–248	Urethane	HS/Estane	
219–225, 261.3	Diphenyl methane	HS/Estane	Estane degradation
270	Ben-NO_2 (nitrobenzene)	HS/Estane	Estane degradation
270–285	>C=O (weak)		NP and Estane degradation
278	BHT derivatives	Irganox	Arm broken off
302	-N=O (nitroso)	NP isomer, HONO	NP addition
205–210, 317	BHT quinone derivative	Oxidized Irganox	Degradation of Irganox
227–229, 272	Benzoic acid (Ben-COOH)	HS/Estane	Degradation of HS
239–241, 308 262, 272, 324	Tetraphenylethene and its derivatives	Oxidized HS/Estane	X-linking at methyl group in diphenylmethane

3.2. Aged HE Samples

3.2.1. Evidence of NP Degradation

Figure 5 (top row) shows UV spectra of NP aged inside the HE samples at 60°C for 4, 12, and 24 months. At 12 months and before, the UV spectra of aged NPs appear to be identical to that of NP aged in the control sample, suggesting insignificant degradation. At 24 months, small changes, such as peak shift, are observed in the aged samples, indicating the onset of NP degradation. Figure 5 (bottom row) shows the UV spectra of NP aged in the HE samples at 80°C for 4, 12, and 24 months. Changes in the UV spectra are observed as early as the first four months. Namely, a new peak emerges at ~302 nm, and is suspected to be associated with the -NO (nitroso) group, likely generated from NP isomerization/degradation through HONO elimination [34]. At 12 months, while the intensity of the NO peak grows further, a new peak emerges at ~285 nm, which may be due to increased concentration of >C=O and -CHO groups. The peak at 231 nm blueshifts to 226 nm in VWHE and WHE, suggesting the presence of NP residuals – nitro-alkene derivatives containing the >C=C(NO_2)- group, which agrees with earlier findings obtained in the Fourier transform infrared (FTIR) spectroscopy studies [12, 32]. Indeed, these nitro-alkene derivatives are the key intermediates in the earlier steps of NP oxidative isomerization/degradation [14, 32, 33]. One of the possible pathways is shown as Reactions (a) and (a') in Figure 6, when HONO or NO_2 radicals are in close proximity with the nitro-alkene derivative, which allows for re-addition through Reactions (b) - (e) before they diffuse away [14]. One might consider that these reactions resemble the addition of H_2SO_4 to an alkene to yield alkyl hydrogensulfate, which is also reversible. One would further expect similar elimination in weak yields from alkylnitrates and nitroalkanes, for the latter a five membered ring intermediate, as shown in an inset in Figure 6, taking advantage of the partial negative charge on the oxygen (in the bonded nitro group) to connect with the neighboring H, which would easily yield HNO_2/HONO from the RCH_2-$C(NO_2)_2CH_3$ molecule [35]. Typically, to form HONO from a nitroalkane, basic catalysis is required. However, when the formed nitro-alkene is a highly electrophilic acceptor, basic catalysis is not needed due to its high reactivity [36].

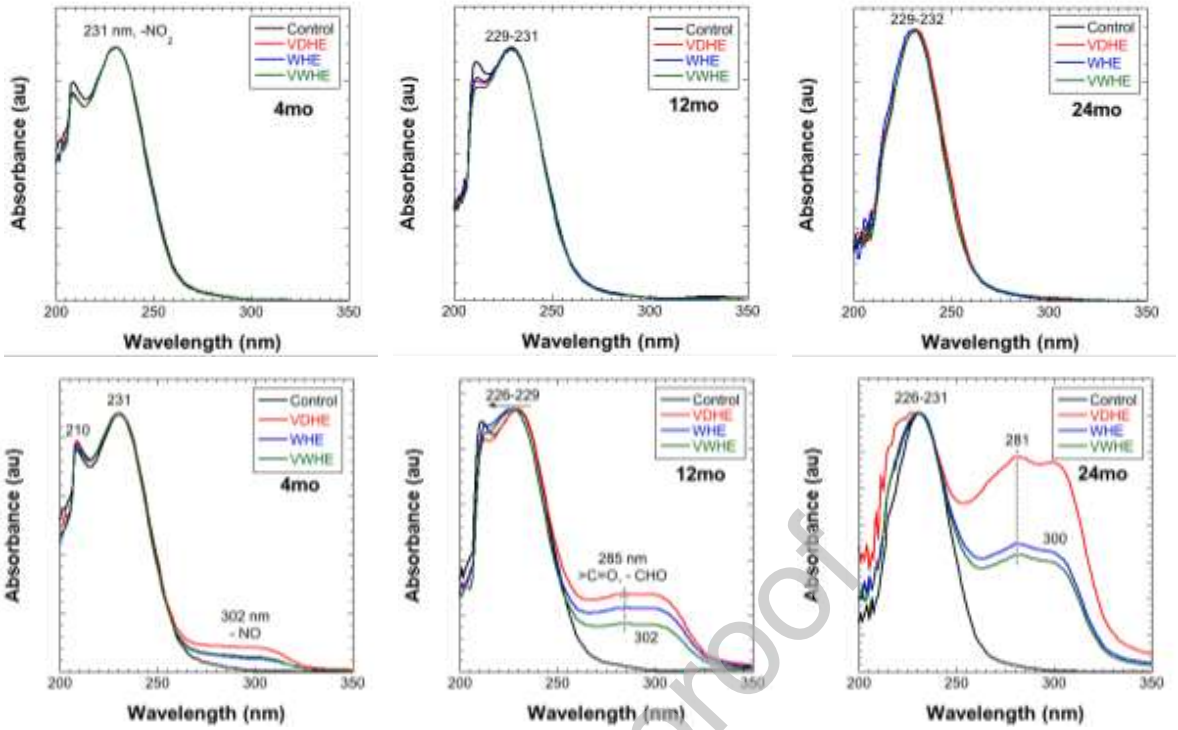

Figure 5. UV spectra of NP aged inside the 60°C (top row) and 80°C (bottom row) samples from 4, 12, and 24 months. All data were normalized to ~230 nm peak of their control samples analyzed at the same ages.

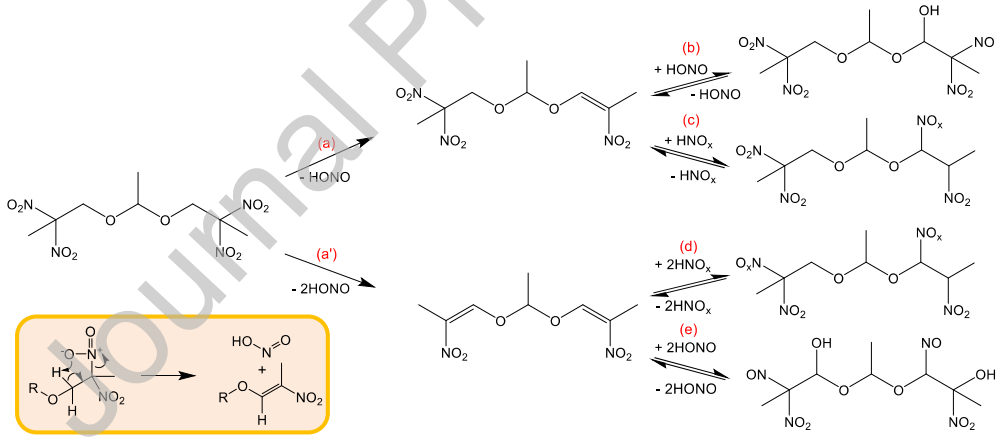

Figure 6. First few possible reactions proposed in the NP degradation process [14, 32]. Products can exist in various isomers though only representatives are illustrated here for brevity. Inset illustrates five-member ring formation as an intermediate step of HONO formation.

On the other hand, one possible reason for the detection of the nitro-alkene derivatives is that elevated temperature accelerates HONO decomposition and HNOx evaporation. This reduces the HONO and/or HNO_x addition through Reactions (b) - (e), and resulting in the accumulation of the nitro-alkene derivatives at 12 months and 80°C. At 24 months, the intensities of the broad peak at ~281 nm and the -NO peak grow significantly compared to the 231 nm peak, suggesting that degraded NP fragments contain not only more >C=O and -NO groups, but also other functional groups, such as -COOH, $-NO_x$, -CHO, which complicate the data interpretation. Nevertheless, most changes are found

in the VDHE sample, implying NP degrades the most under dry conditions, which agrees with the previous findings [11, 12, 32, 33]. After 24 months of aging at 80°C, NP completely degrades regardless dry or wet condition, confirming poor thermal stability of NP at the elevated temperatures.

3.2.2. *Evidence of Estane Oxidation*

Considering the least possibility of hydrolysis occurring in the driest sample, Figure 7(a) and (b) illustrate how the UV spectra of Estane aged in the VDHE samples change over time at 60°C and 80°C, respectively. At 60°C, changes in the region between 280 nm and 350 nm emerge after 12 months. Since they have never been observed in hydrolyzed Estane, these changes provide the evidence of NP addition, namely the presence of -NO group in the aged sample [37]. NP addition and/or Estane oxidation degradation is only at their early stage at 60°C after 24 months of aging. Since the peak of the hard segments at 248 nm is intact, oxidation most likely takes place in the ester (-COO-) and even urethane (-NH-COO-) groups, but not at the methyl bridge between two phenyl rings. Since HONO decomposition will generate water, it is also expected that hydrolysis occurs as well when NP degrades.

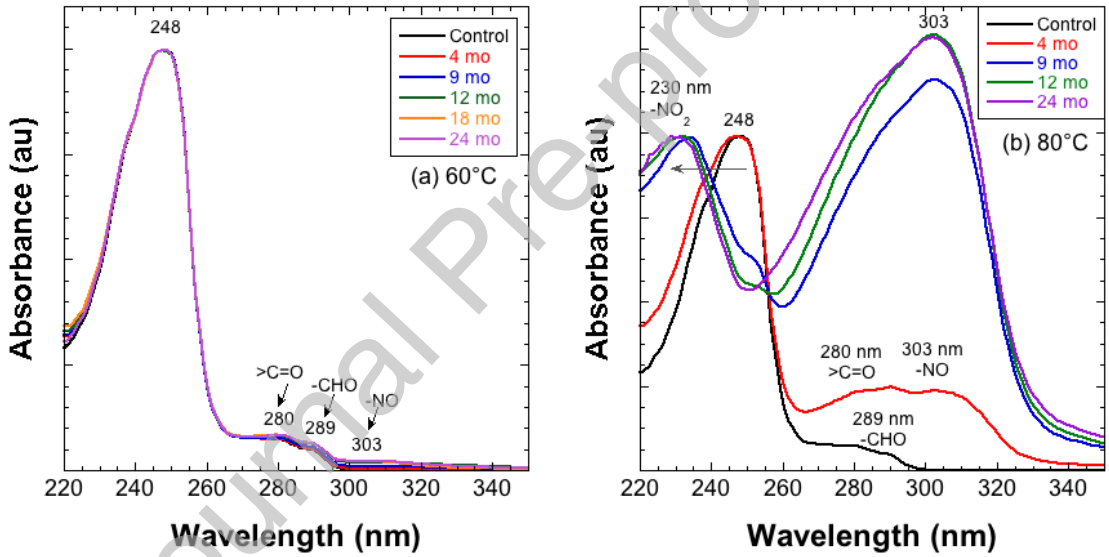

Figure 7. UV spectra of Estane samples aged inside the VDHE samples at 60°C (a) and 80°C (b) for two years. The UV spectra were collected from the apexes of the GPC elugrams. The peak between 220 nm and 250 nm of the aged samples were normalized to the 230 nm peak of the control sample.

At 80°C, the UV spectrum of Estane completely changes over time, as shown in Figure 7(b). The hard segment peak at 248 nm disappears gradually and is eventually replaced by the peaks around 230 nm. Simultaneously, a new peak at 303 nm and shoulder at ~280 nm eventually outgrows the 248 nm peak. All of these changes suggest the oxidation of Estane occurring in both soft and hard segments at much more aggressive rate at 80°C than at 60°C. In the NP environment, the methyl bridge in hard segments was oxidized into carbonyl group (>C=O), which has been documented in numerous papers when the techniques of the gas chromatography mass spectrometry (GCMS) and N^{15} and C^{13} labelling nuclear magnetic resonance (NMR), and conventional GPC were implemented to analyze the aged HE samples at various conditions [1, 7, 19, 38, 39]. In addition to the oxidation, ring nitration could be another possible degradation pathway occurring in the hard segments. However, the N^{15} labelling

NMR study suggests the occurrence of the ring nitration is insignificant when the aging temperatures are below 70°C for a few months [38]. On the other hand, the presence of -NO and -NO_2 groups in the aged Estane and the large growth of the broad peak between 260 nm and 340 nm, suggesting that degraded NP fragments react with aged Estane through NP addition reactions. The exact reaction pathways are under investigation. Nevertheless, the UV spectrum of the aged NP and Estane, which can be readily obtained from a GPC equipped with a PDA detector, is rarely reported, but should be used as an effective technique to detect oxidation in the PBX 9501 aging study.

Figure 8 (and Figure S2) shows detailed GPC elugrams obtained from three detectors for the 60°C samples aged from 9 to 24 months. More detailed discussion is given in Supplementary materials. The key findings are: 1) the intensity of the Irg1010 peak decrease strongly in all samples within the first four months, and completely disappears in the VDHE sample at 9 months, and in the other two samples at 12 months, suggesting the generation of oxidants in the aged samples and more oxidants is found in VDHE than in the other two samples; 2) for the first four months, except for a slight change in peak width and retention time, the GPC elugrams are similar to each other among all samples regardless of different GPC detectors, and show a Gaussian-like distribution. A small increase in intensity is observed in the low molecular weight (LMW) region from the DRI signal, but less so in the PDA and MALS (its intensity depending on molecular weight) signals, suggesting that the degraded products are most likely comprised of soft segments (weak UV signature) and generated through ester hydrolysis; 3) at 12 months, as Irg1010 depletes, the radicals from NP degradation are able to attack Estane through oxidation. The GPC elugrams of all HE samples start to deform from Gaussian distribution, as shown in the 2nd vertical strip of Figure 8 (and Figure S2). For all samples, the signals of the formed high molecular weight (HMW) and LMW materials are observed, but to different extents. The HMW materials are likely due to the formation of cross-linked (X-linked) segments through the oxidation of the methyl bridge in diphenyl methane [7, 8, 19] whereas the LMW materials are likely due to chain scission through ester hydrolysis and oxidation [6, 19, 40]; 4) at 18 months and after, the LMW region grows the most in VDHE, resulting in the lowest molecular weight. On the contrary, an appreciable amount of HMW material in the VWHE and WHE samples is continuously formed, leading to the observed poor solubility. Since the most deformed peak is found in VDHE, we conclude that Estane was oxidized most in VDHE, implying that NP degrades the most under the dry conditions and explaining the high depletion rate of Irg1010 in this driest sample.

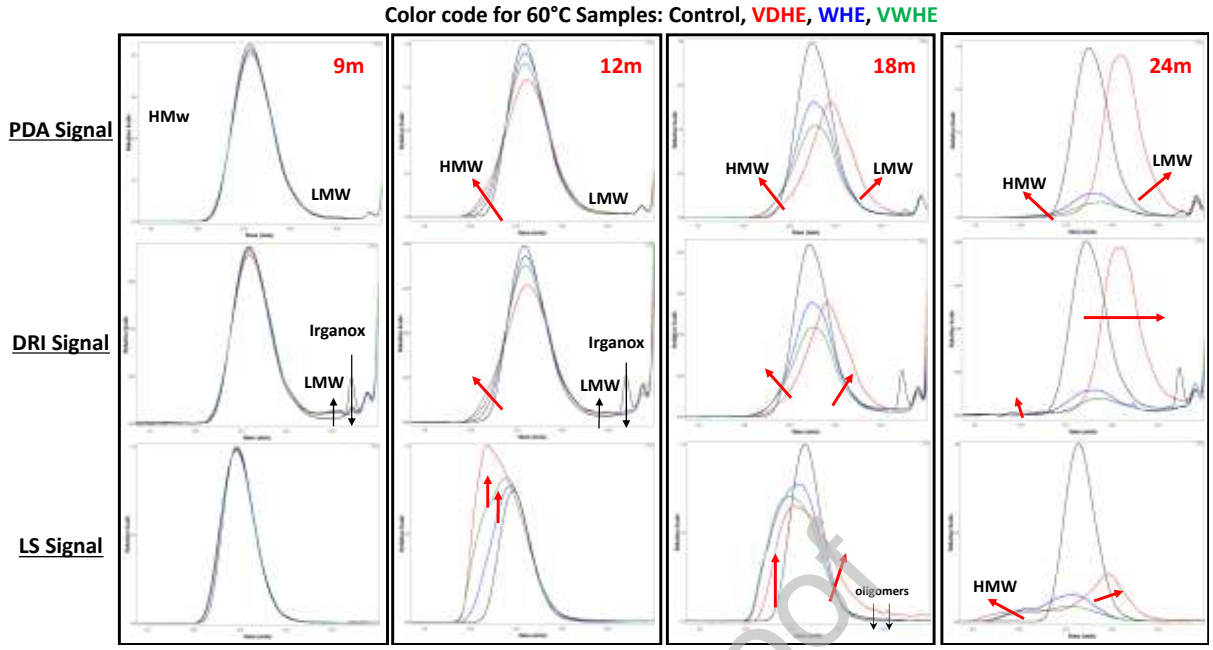

Figure 8. GPC elugrams of the 60°C samples aged at various conditions. UV signals are obtained from the PDA detector set at 250 nm, and LS signals are from the MALS detector at 90° angle. The red arrows indicate the concentration increase and abnormal changes in the GPC signals.

Figure 9(a) shows the M_w as a function of time for the 60°C samples. Within the first four months, the changes in M_w are not significant, owing to the protection of Irg1010 from the oxidant attack and even hydrolysis. At 9 months and after, the M_w starts to fluctuate over time. Apparently, the formation of the HMW material through oxidation is more predominant than the formation of LMW material through chain scission by hydrolysis and/or oxidation, the M_w of three samples increases between 9 and 12 months (even 24 months for WHE). After 12 months and later, the M_w of VDHE significantly decreases and reaches the lowest value (<30 kDa) at 24 months, suggesting that Estane degrades the most in VDHE. On the contrary, the M_w of WHE and VWHE exhibit different behaviors, evidencing the complex dependence of degradation mechanisms on their initial water concentrations.

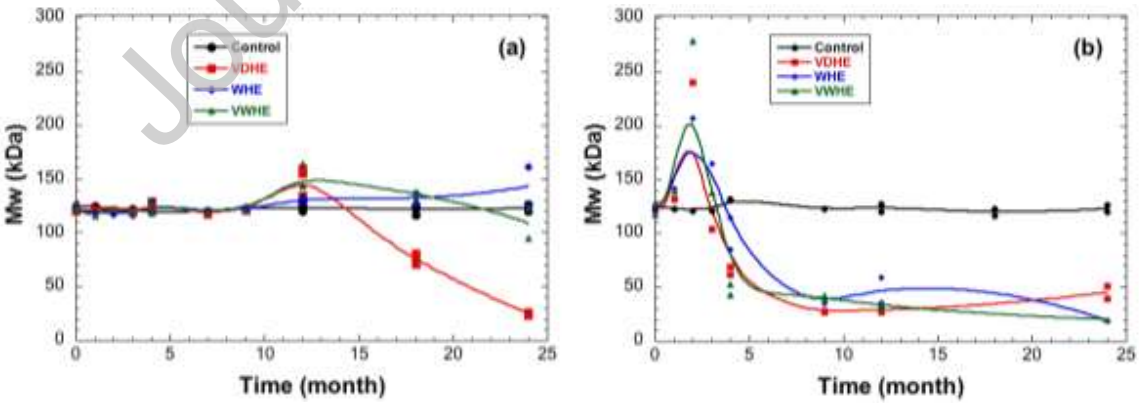

Figure 9. Effect of aging on the M_w of (a) the 60°C samples and (b) the 80°C samples. Data obtained from the DRI detectors from two laboratories.

Figure S3 shows detailed GPC elugrams for the 80°C samples aged from 4 to 24 months. The key findings are similar to those obtained from the 60°C samples, but changing at a much faster rate.

Notably, the GPC elugrams start to deviate from Gaussian distribution before four months. Evidentially, Irg1010 was completely consumed within two months according to the HPLC results and an appreciable amount of HMW materials was detected for all the samples. As aging progresses to 9 months and beyond, the GPC elugrams of the aged Estanes show the following changes: 1) shift toward longer retention time; 2) become wider and further deviate away from Gaussian distribution; and 3) change from single modal to bi-modal or even tri-modal distribution. Figure 9(b) shows the M_w of the 80°C samples as a function of time. The increased M_w is observed at as early as the first two months, and then M_w sharply decreases after two months. At 9 months and after, the M_w reaches a pseudo-plateau at and below 50 kDa. All these GPC results confirm that Irganox, NP, and Estane are significantly degraded in these HE samples through multiple mechanisms when aged at 80°C.

3.2.3. Effect of Water Concentration on NP and Estane Degradation

The aforementioned UV and GPC results have shown that the aging behaviors of these three HE sample types are significantly different. The key factor to cause this difference is their initial water concentration. Based on water gained in the preconditioning process, VWHE is expected to contain ~115 ppm more water than WHE, and ~330 ppm more water than VDHE. Considering only 5 wt% binder in PBX 9501, the 330 ppm difference in the HE sample could lead to as much as 6600 ppm difference in the binder material based on the assumption that water absorption is much lower in HMX compared to the binder materials [21].

Previously, we postulated that NP degrades differently under differing humidity conditions, as shown in Figure 2 and in the center of Figure 10. Dry vs. wet conditions lead to NO_x dominant or HNO_x dominant products, which trigger both NP residuals and Estane to degrade through different reaction pathways, as conceptually illustrated in Figure 10. Furthermore, temperature alters these pathways, thus the resultant molecular weight and chemical properties of aged Estane. For instance, while hydrolysis results in the monotonic decay of molecular weight over time, as highlighted inside the green boxes, oxidation and NP addition can lead to fluctuations in the molecular weight over time. Often, since more than one degradation mechanism can be active simultaneously, the actual changes in the molecular weight of Estane are expected not to follow a simple or monotonic trend. Therefore, the molecular weight will not sufficiently describe the properties of the polymer. Chemical characterization, such as UV, FTIR, and NMR spectroscopy, is essential to reveal the structural change in the aged polymer. The detailed degradation mechanisms of NP and Estane are currently being studied and will be reported in subsequent papers.

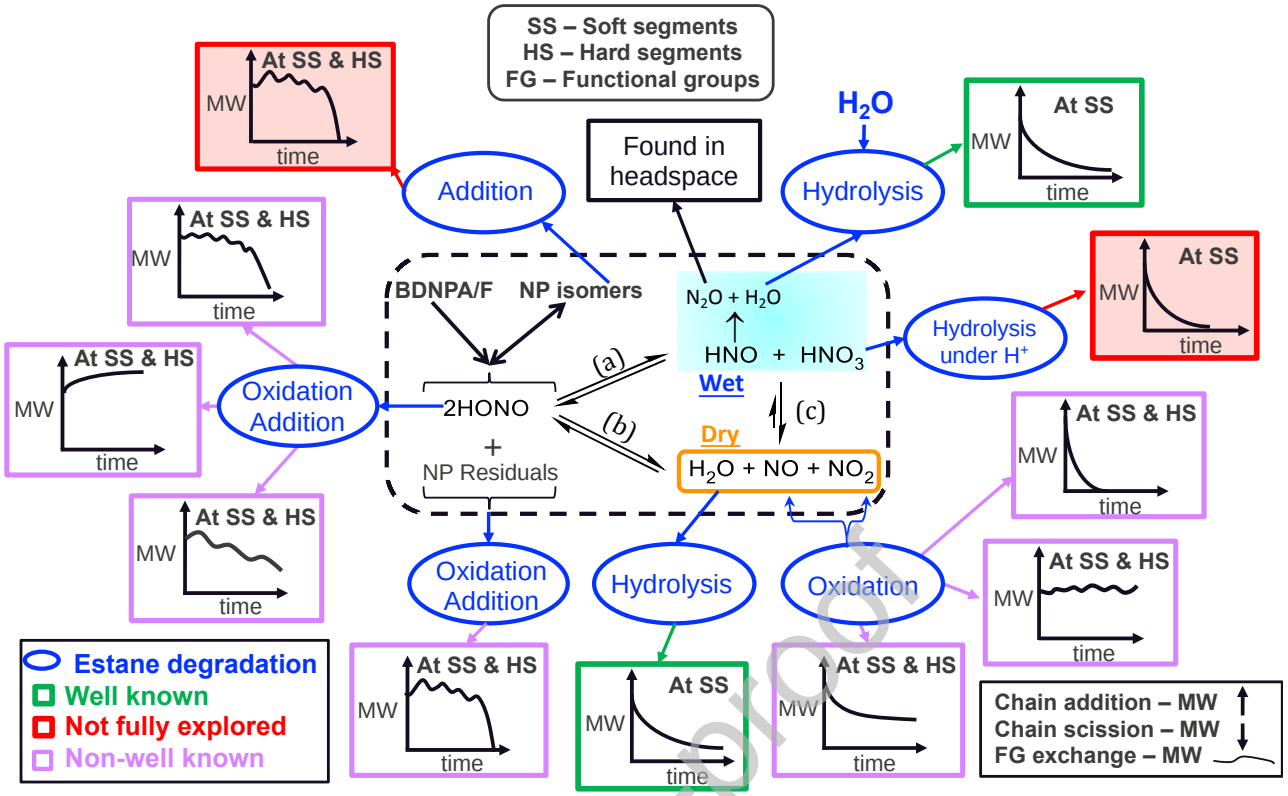

Figure 10. Impacts of aging conditions on the postulated degradation pathways of NP on the early stage and Estane and thus on the molecular weight (MW) of Estane aged in PBX 9501.

It is worth noting that since the compounds - BDNPA/BDPNF in NP are acetals, it is expected that acidic molecules serve as catalysts to hydrolyze NP at -O-C-O- group [20, 41, 42] when water and acid concentrations are sufficiently high, which often occurs at the late stages of thermal aging of NP [12, 34, 43]. Compared to volatile molecules produced through NP degradation: NO_x, HNO_x, formaldehyde, acetaldehyde, and carboxylic acid [12, 32], the product from BDNPA/BDNPF hydrolysis – 2,2-dinitropropan-1-ol (DNPOH) and DNPOH derivatives, is rather stable and can form hydrogen bonds among themselves and other polar molecules [44]. As expected, they often stay in the condensed phase and could be detected as key final products in the PBX 9501 and other nearby components after a long-term in service. Still, the small molecules, like H_2O, NO_x, and HNO_x, generated from HONO degradation can be more detrimental to the stability of Estane and NP than DNPOH and its derivatives, as these small molecules can serve as both reactants and catalysts. For the latter role, a trace amount of them can accelerate the degradation of Estane significantly.

3.3. Role of Antioxidant in PBX 9501 Aging

Due to the oxidative environment generated by NP degradation, the role of the antioxidant is vital in the stabilization the components in PBX 9501. Although PBNA was added into NP after its production, its concentration is close to detection limit after a few decades of storage. On the other hand, Irg1010 (0.1 wt%) was added into PBX9501 production, its concentration was monitored in this study. More discussion is warranted on how Irg1010 degrades during the PBX 9501 aging and on how the aging condition affects its consumption rate.

3.3.1. UV Spectra of Irg1010 Aged in the 60°C Samples

Figure 11 shows the UV spectral change of Irg1010 over time when the HE samples were aged at 60°C. The UV spectrum of pristine Irg1010 exhibits two distinct peaks, at 209 nm and 278 nm, which are associated with $C(\text{-}CH_2OO\text{-})_4$ and BHT groups, respectively. When an oxidant attacks Irganox, quinone-type structures form to stabilize the system by resonance in Reactions (b1, b2), which is responsible for the peak at 317 nm in the UV spectra of oxidized Irg1010 [30, 31]. These structures have the ability to further trap other peroxyl and NO_x radicals, as shown in Reactions (a, c_1, c_2, c_3) of Figure 12 (left). Irg1010 could also undergo acid-catalytic hydrolysis at the ester groups, as shown in Figure 12 (right), which impairs the ability of Irg1010 to stabilize the quinone structures formed after the phenyl rings absorb radicals [45]. In PBX 9501, radicals (NO_2• and NO•) and HNO_x generated from NP degradation will attack Irg1010. As a result, the intensity of the 209 nm peak decreases in all samples over time, suggesting that the $(\text{-}CH_2OO\text{-})$ moiety is acid-catalytically hydrolyzed sequentially to form pentaerythritol $[C(\text{-}CH_2OH)_4]$. Accordingly, a shoulder grows at ~231 nm, which might be attributed to the $\text{-}NO_2$ group added into degraded Irg1010 through Reaction c_1 of Figure 12 (left). As quinone forms through Reaction ($c_{1\text{-}2}$), the intensity of the peak at ~317 nm increases relative to the intensity of the main peak at 209 nm.

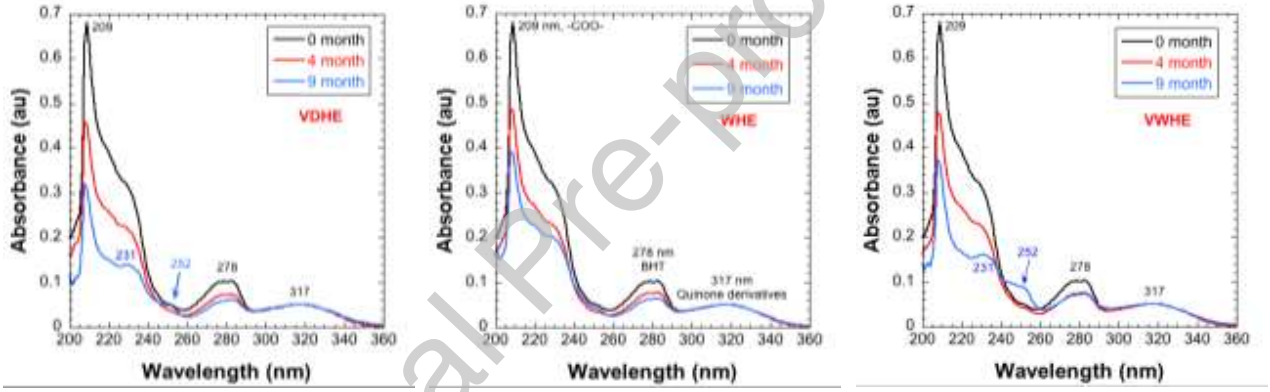

Figure 11. UV spectra of Irg1010 aged inside three HE samples at 60°C during aging process. The spectra were normalized over the 317 nm peak.

Another interesting observation is a ~252 nm peak formation. It is reported that both BHT-COOH and BHT-quinone (BHT-Q) give an absorbance at ~256 nm in methanol [46]. We suspect that the same compounds are found here and the 4 nm difference may be due to the solvent effect (THF vs. methanol). By following the reaction pathway proposed in Figure 13, the arms of Irg1010 are broken off through ester hydrolysis, followed by the NO_x radical attack at OH-groups to form BHT-COOH or BHT-Q depending on the humidity. Among three samples, the VWHE sample gives the highest intensity at ~252 nm peak, suggesting most formation of the BHT-COOH is due to its highest water concentration among three samples. Conversely, due to the least water concentration in VDHE, the peak ~252 nm peak is likely associated with the BHT-Q compound. As expected, both oxidation and hydrolysis impair the efficiency of Irg1010 when aged inside PBX 9501.

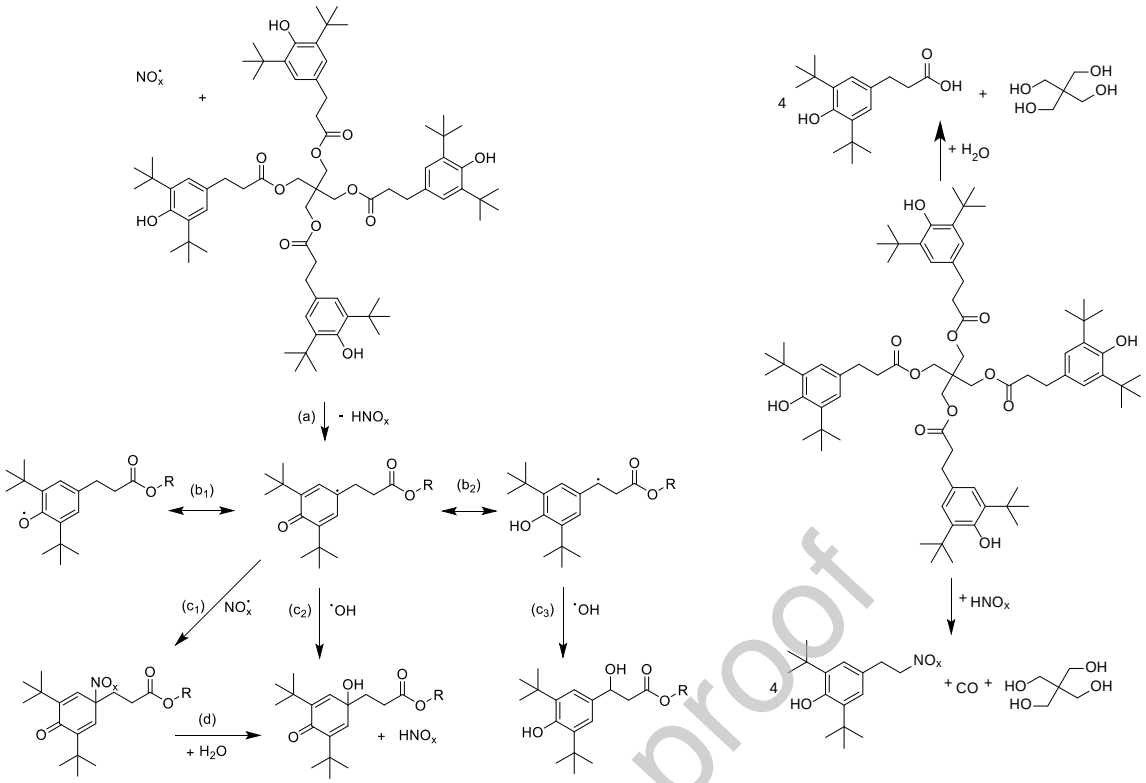

Figure 12. Proposed oxidation mechanism for Irg1010 (left – modified from reference [10]) and hydrolysis mechanism through HNO_x addition for Irg1010 (right).

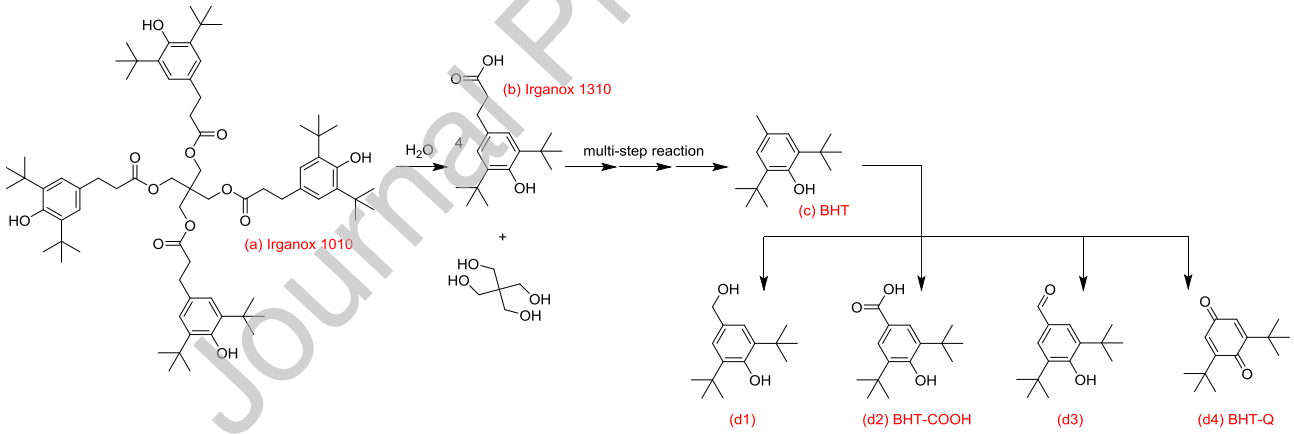

Figure 13. Proposed reaction pathway of Irg1010 oxidation (modified from Tao et al. [46]). The figure includes a multi-step reaction between products (b) and (c) due to uncertainty in the mechanics of this reaction.

3.3.2. Irg1010 Consumption in Aged HE Samples

Figure 14 compares the similar trends among concentration of Irg1010 obtained from HPLC and GPC as a function of time for the 60°C samples. The initial concentration of Irg1010 in the VDHE, VWHE, and control samples were measured to be 0.060, 0.063, and 0.068 wt%, respectively, which are less than the expected value (0.1 wt%) suggesting, as discussed in Section 3.1.2, that some Irg1010 was already consumed during preconditioning process. Still, the concentration of Irg1010 decreases at the fastest rate in the VDHE sample. The excess amount of water in VWHE would cause the suspected

hydrolysis of Irg1010 [10]. However, the depletion rate of Irg1010 in VWHE is slower than that in VDHE, suggesting most oxidants were generated in the VDHE sample. Among the three conditions, Irg1010 decreases at the slowest rate in the WHE sample at 60°C.

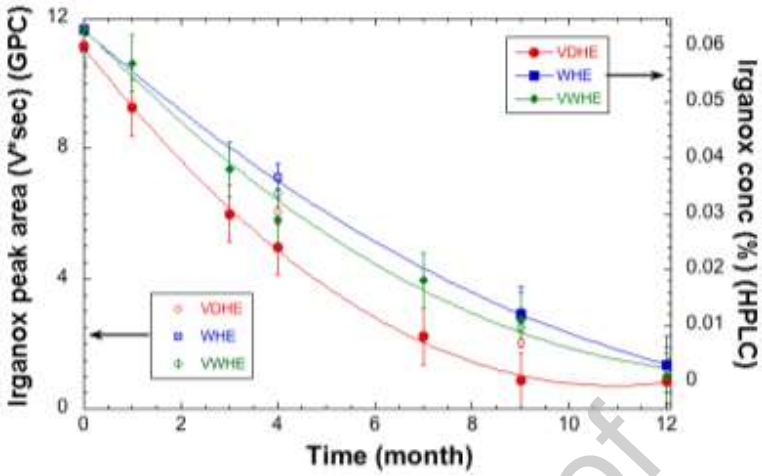

Figure 14. Measured concentration of Irg1010 in 60°C samples, as analyzed by both GPC and HPLC.

Figure 15 correlates the trends between Irg1010 concentration vs. time and M_w of Estane vs. time when the HE samples were aged at 60°C for two years. As Irg1010 concentration approaches zero, NP degrades noticeably (< 10 wt%), and Estane degrade significantly. While Estane degradation manifests as large changes in its molecular weight, NP degradation manifests as a decrease in its concentration in HE samples [24]. The results demonstrate that Irg1010 plays a critical role in scavenging oxidant/radical species generating in PBX 9501.

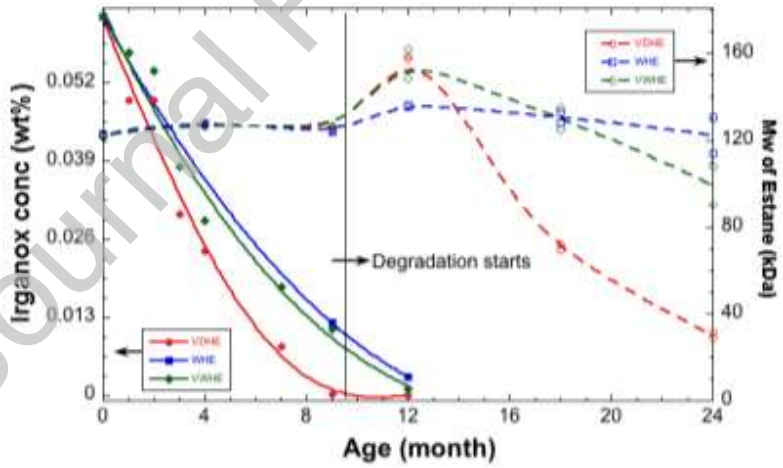

Figure 15. Effect of Irg1010 consumption on the molecular weight of Estane in the 60°C samples as a function of time.

For the 80°C samples, the concentration of Irg1010 was not measured after two months as it was below detection limit in all samples, signifying that the depletion rate of Irg1010 is at least 6 times faster at 80°C than at 60°C. Based on this ratio, Arrhenius law ($k_1/k_2 = \exp [-E_a/R*(1/T_1 - 1/T_2)$, T in K and R = 8.314 kJ/(mol.K)] was used to estimate the activation energy (E_a) for Irg1010 consumption when aged in PBX 9501. The estimated E_a is 87–89 kJ/mol, which is remarkably close to the value of 85.8 kJ/mol reported by Salazar et al. in 2009 for the Estane aging in PBX 9501 up to 64°C [19]. These

results indicate that a common degradation mechanism in these different studies drives the degradation of PBX 9501, which most likely involves NP degradation.

3.3.3. Predication of Irg1010 Consumption in PBX 9501

3.3.3.1. Under wet environment

Using the Arrhenius expression [k(1/day)=exp(24.834–76688/RT)] for the hydrolyzation of Irg1010 [10] its consumption can be predicted at different temperatures, as shown in Figure 16. Assuming the Irg1010 undergoes hydrolytic degradation, its lifetime would be significantly less than the data obtained in this study. For example, complete depletion of Irg1010 in the PBX 9501 samples is only achieved after 12 months at 60°C and 2 months at 80°C, which are much longer than the prediction given in the plot. This implies that hydrolysis is not the only mode of the degradation for Irg1010 consumption, and the analysis in the PBX 9501 sample still shows the presence of antioxidant even after three decades in service life. Thus, the Arrhenius prediction from ref [10] is not strictly applicable for Irg1010 aging in PBX 9501.

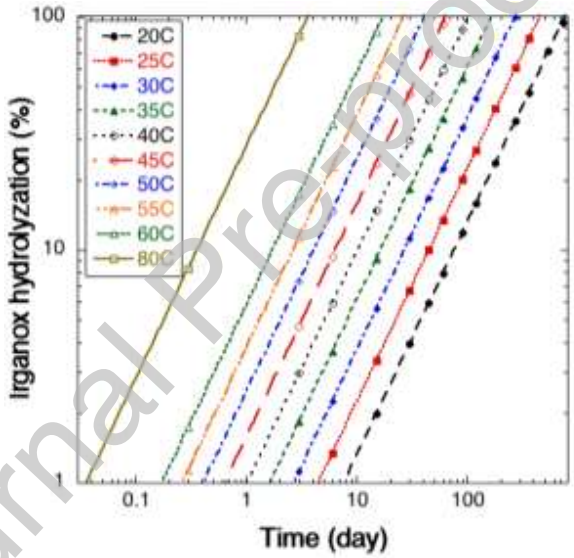

Figure 16. Predicted Irg1010 hydrolyzation rate over time at various temperatures using Arrhenius law given in ref [10].

3.3.3.2 Under dry environment

In the scarce water condition, as NP degrades through HONO elimination, as shown in Reaction (b) in Figure 2, Irg1010 is primarily consumed by NO_x. Using the Arrhenius law ([product]=k*t*$[NP]_0$, k(1/day)=1.27x10^{22}*exp(-170500/RT), $[NP]_0$=4.356 mol/L) for this elimination reaction [11], the generation of oxidants (NO_x = NO +NO_2) can be predicated at different temperatures, as shown in Figure 17(a). This prediction provides an estimated timeline of Irg1010 consumption in the PBX 9501 samples, assuming Irg1010 is fully consumed when the concentration of NO_x is equal to that of Irganox. In this study, the HE samples initially contain 0.06 wt% Irg1010 and 2.40 (± 0.05) wt% NP, hence, the concentration of Irg1010 in NP is 0.03 (mol/L) at time zero. Considering four-fold efficiency, the effective concentration of Irg1010 as the antioxidant agent is 0.12 (= 4x0.03) (mol/L), as shown with the black line in Figure 17(a). Depending on the aging temperature, the amount of

generated NO_x would not sufficiently consume Irg1010 for at least 50 years at 40°C or below, ~12 months at 60°C, and < 2 months at 80°C, respectively, which agree with the experimental results reasonably well in the current study.

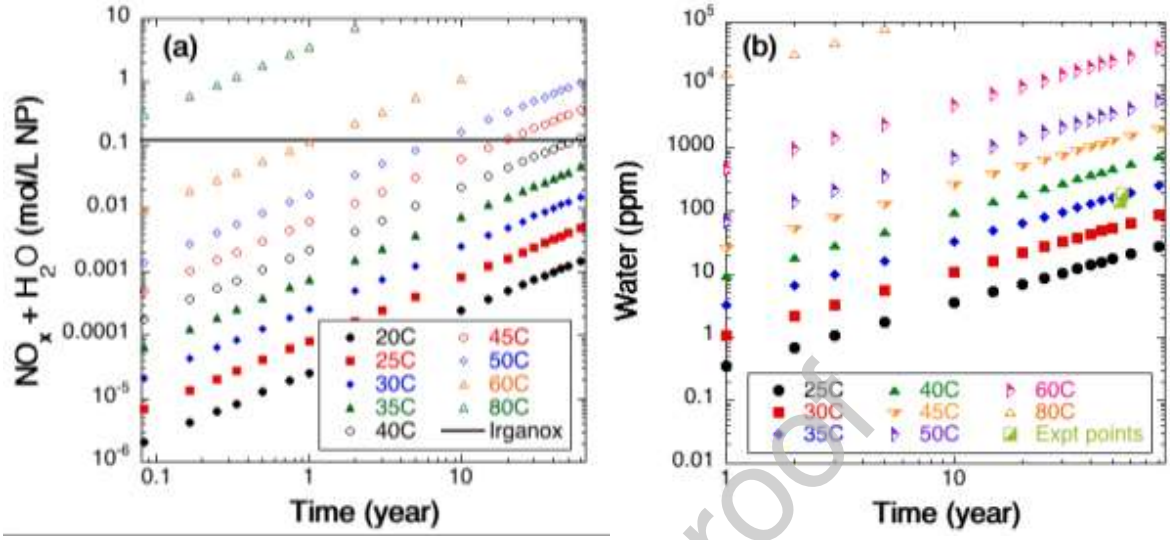

Figure 17. Prediction of $NO_x + H_2O$ (a) and water (b) generated from the HONO decomposition as a function of time and for various temperatures. 0.06 wt% of Irg1010 in the HE samples, as indicated by the black line.

Furthermore, using Figure 17(b), water generation can be estimated at various temperatures as well. Specifically of interest in the current study, it is found that 483 ppm and 15768 ppm water could be generated in NP at 60°C and 80°C within one year, respectively. They are equivalent to 12 ppm and 394 ppm gained in PBX 9501, accordingly. Whereas the extra 12 ppm of water in the HE sample is not significant compared to the initial water concentration in VWHE (~389 ppm) and WHE (~275 ppm), the extra 394 ppm of water in the HE sample is substantial. As expected, once NP degrades greatly, the products like H_2O, NO_x, HNO_x, and NP residuals will aggressively degrade Estane, NP itself, and Irg1010 through complicated reaction pathways.

Conversely, at ambient conditions, the overall increase in the water concentration of NP is minimal. After ~55 years of storage, it was found that the concentration of water was between 700 and 800 ppm (mass/mass), which is up to 100-200 ppm higher than that in its pristine form (~600 ppm) [11, 47]. Actually, increased water concentration is expected. While the generated NO_x radicals from HONO decomposition can be scavenged by PBNA and its derivatives (PBNA + xNO_2, x = 1-3), water starts to accumulate. The increased water concentration also matches the prediction value assuming that the storage temperature is below 30°C. As PBNA and its derivatives deplete, NO_x will react with water to form HNO_x, which results in the increased acidity. These results explain the full consumption of PBNA after a long-term storage.

It is worth noting that there might be some discrepancies between the theoretical predication and experimental results under different humidity conditions. The possible reasons are that: 1) Irg1010 is not four-fold efficient as expected; 2) the amount of oxidant species could be underestimated if NP degradation progresses beyond the HONO elimination stage and other components in PBX 9501 could generate oxidant species at elevated temperatures; and 3) acid-catalytic hydrolysis can play an

important role in degrading Irg1010 as the water concentration and the acidity largely increase due to the aggressive NP degradation at elevated temperatures.

4. Conclusions

A set of HE samples with different initial water contents aged at 60°C and 80°C has been systematically characterized. Although the samples were labelled "very dry", "wet", or "very wet", their water contents actually differed by less than 400 ppm. Yet, this <400 ppm difference was sufficient to significantly alter the aging behavior of Irg1010, NP, and Estane in PBX 9501. Without extra caution, these few hundred ppm of water can be easily overlooked. This might explain why the role of water in the stability of PBX 9501 has never been studied in such great detail.

To study the aging behavior of the blend materials in PBX 9501, extra care must be applied because NP degradation is sensitive to both water and temperature. Furthermore, many products from NP degradation are volatile and it has been shown that NP degradation is more sensitive to headspace under dry conditions than wet conditions [12]. The results shown here also support that while water can readily hydrolyze Estane, a trace amount of water can slow down the decomposition of NP. Alternatively, under ultra-dry conditions, the generated NO_x and even ozone (potentially generated from chemical reactions between NO_x and volatile organic compounds) will work together with water to attack Estane and NP through much more complicated mechanisms, which is especially true at elevated temperatures.

Regardless of humidity and temperature conditions, an antioxidant, such as Irganox, will serve as a scavenger to protect NP and Estane from the attack of oxidants/radicals, such as NO_x, through oxidation and/or from the attack of water and acidic molecules, such as HNO_x, through acid-catalytic hydrolysis. Therefore, the stabilizer plays a vital role in thermal stabilization of the PBX 9501. It is also worth noting that, Irg1010 is designed for scavenging oxygen (biradical), but not as effective at scavenging radicals by comparison. In the NP environment where NO_x are generated over time, common stabilizers, like diphenylamine, PBNA, Acardite II, etc. should be considered as suitable alternatives to Irg1010.

Furthermore, to characterize the molecular weight of the binder materials, a GPC equipped with a DRI detector has been used for many years. While this conventional GPC technique can adequately analyze hydrolyzed Estane, it becomes obsolete to analyze the polymer after undergoing more complex degradations, such as Estane aged in PBX 9501. Therefore, the multi-detection GPC technique is an excellent replacement and will provide more informative insights on the chemical structure changes in aged Estane.

Credit authorship contribution statement

Dali Yang: Conceptualization, Methodology, Formal GPC and UV analyses, Writing – original draft, review, and editing, Supervision. ; David A. Upshaw: Experiment design, execution, and supervision, Writing – review & editing. ; Alexander S. Edgar: NP and Irganox degradation chemistry, Writing – review & editing. ; Christopher J. Rosales: Conventional GPC and HPLC analyses.

Declaration of Competing Interest

All authors do not have any financial or personal relationships that may be perceived as influencing their work.

Acknowledgments

We thank Mike Steinzig who managed the entire project and the execution of the project; Devin Booker for his assistance with experimental design, HE sample preparation, and execution; Adelaida Valdez for the preparation and pressing of the HE samples; Geoff Brown for helping on the aging experiment in many aspects; Racci Deluca for crushing the HE samples; Anne Giambra for the preparation of the GPC and HPLC solutions and the analyses of Estane, NP, and chemical minors in the early stage of this project. We thank Troy Holland, Julie Jung, Joel Kress, Cameron Moore, Paul Peterson, Ruilian Wu, Robert Gilbertson, Michael Blair, and Chris Freye for fruitful discussions on the topic of PBX 9501 and NP degradation. This work was supported by the US Department of Energy through the Los Alamos National Laboratory Aging and Lifetimes Program. Los Alamos National Laboratory is operated by Triad National Security, LLC, for the National Nuclear Security Administration of U.S. Department of Energy (Contract No. 89233218NCA000001).

5. References

[1] D. Wrobleski, D. Langlois, E. Orler, D. Dattelbaum, J. Small, Application of 15N labeling for oxidative degradation study of a plasticized poly(ester urethane), Polymer Preprints 45(1) (2004) 2.

[2] M.R. Salazar, R.T. Pack, Degradation of a Poly(ester urethane) Elastomer. II. Kinetic Modeling of the Hydrolysis of a Poly(butylene adipate), J. of Polymer Science: Part B: Polymer Physics 40 (2002) 8.

[3] M.R. Salazar, S.L. Thompson, K.E. Laintz, R.T. Pack, Degradation of a Poly(ester urethane) Elastomer. I. Absorption and Diffusion of Water in Estane 5703 and Related Polymers, J. of Polymer Science: Part B: Polymer Physics 40 (2002) 181-191.

[4] M. Geisler, T.S. Pal, K. Arnhold, M. Malanin, M.T. Muller, B. Voit, J. Pionteck, A. Lederer, Impact of Electron Beam Irradiation on Thermoplastic Polyurethanes Unraveled by Thermal Field-Flow Fractionation, Polymer Degradation and Stability (2020).

[5] D. Idar, D.G. Thompson, G.T.G. III, W.R. Blumenthal, C.M. Cady, P.D. Peterson, E.L. Roemer, W.J. Wright, B.J. Jacquez, Influence of Polymer Molecular Weight, Temperature, and Strain Rate on the Mechanical Properties of PBX 9501, Shock Compression of Condensed Matter, American Institute of Physics Publishing, 2002, p. 5.

[6] M.R. Salazar, J.M. Lightfoot, B.G. Russell, W.A. Rodin, M. McCarty, D.A. Wrobleski, E.B. Orler, D.A. Spieker, R.A. Assink, R.T. Pack, Degradation of a poly(ester urethane) elastomer. III. Estane 5703 hydrolysis: Experiments and modeling, Journal of Polymer Science, Part A: Polymer Chemistry 41(8) (2003) 1136-1151.

[7] M. R. Salazar, J.D. Kress, J.M. Lightfoot, B.G. Russell, W.A. Rodin, L. Woods, Experimental Study of the Oxidative Degradation of PBX 9501 and its Components, Propellants, Explosives, Pyrotechnics 33 (2008) 20.

[8] D.A. Wrobleski, D.A. Langlois, E.B. Orler, A. Labouriau, M. Uribe, R. Houlton, J.D. Kress, B. Kendrick, Accelerated Aging and Characterization of a Plasticized Poly(ester urethane) Binder, in: M.C. Celina, J.S. Wiggins, N.C. Billingham (Eds.) 233rd National Meeting, American Chemical Society, Polymer Degradation and Performance, Chicago, IL, 2009, p. 16.

[9] D.W. Brown, R.E. Lowry, L.E. Smith, Kinetics of Hydrolytic Aging of Polyester Urethane Elastomers, Macromolecules 13 (1980) 5.

[10] S. Beißmann, M. Stiftinger, K. Grabmayer, G. Wallner, D. Nitsche, W. Buchberger, Monitoring the degradation of stabilization systems in polypropylene during accelerated aging tests by liquid chromatography combined with atmospheric pressure chemical ionization mass spectrometry, Polymer Degradation and Stability 98 (2013) 7.

[11] D. Yang, D.Z. Zhang, Role of water in degradation of nitroplasticizer, Polymer Degradation and Stability 170 (2019) 11.

[12] D. Yang, A. Edgar, J. Torres, J. Adams, J.D. Kress, Thermal stability of a eutectic mixture of bis(2,2-dinitropropyl) acetal and formal: Part C. Kinetic Compensation Effect, Propellants, Explosive, Pyrotechnics 45 (2020) 14.

[13] C.F. Melius, M.C. Piqueras, Initial Reaction Steps in the Condensed-Phase Decomposition of Propellants, The Combustion Institute, 2002, pp. 2863-2871.
[14] D.K. Pauler, N.J. Henson, J.D. Kress, A mechanism for the decomposition of dinitropropyl compounds, Physical Chemistry Chemical Physics 9(37) (2007) 5121-5126.
[15] C. Zhao, Y. Chi, Q. Yu, X. Wang, G. Fan, K. Yu, Comprehensive Study of the Interaction and Mechanism between Bistetrazole Ionic Salt and Ammonium Nitrate Explosive in Thermal Decomposition, J. of Physical Chemistry C 123 (2019) 9.
[16] R.S. Booth, C.-S. Lam, M.D. Brynteson, L. Wang, L.J. Butler, Elucidating the Decomposition Mechanism of Energetic Materials with Geminal Dinitro Groups Using 2‐Bromo-2-nitropropane Photodissociation, Journal of Physical Chemistry A 117 (2013) 17.
[17] T.B. Brill, P.E. Gongwer, G.K. Williams, Thermal Decomposition of Energetic Materials. 66. Kinetic Compensation Effects in HMX, RDX, and NTO, J. Phys. Chem. 98 (1994) 6.
[18] F. Minisci, Free Radical in Biology and Environment, Springer Netherlands, 1997.
[19] M.R. Salazar, J.D. Kress, J.M. Lightfoot, B.G. Russell, W.A. Rodin, L. Woods, Low-temperature oxidative degradation of PBX 9501 and its components determined via molecular weight analysis of the Poly[ester urethane] binder, Polymer Degradation and Stability 94(12) (2009) 2231-2240.
[20] C. Freye, C. Snyder, Decomposition of BDNPA/F (NP) Accelerated Aging and Stockpile Aging: Acid Catalyzed Hydrolysis, Presented in an internal meeting, Los Alamos National Laboratory, May 2021, p. 89.
[21] M.R. Salazar, S.L. Thompson, K.E. Laintz, T.O. Meyer, R.T. Pack, Degradation of a poly(ester urethane) elastomer. IV. Sorption and diffusion of water in PBX 9501 and its components, Journal of Applied Polymer Science 105 (2007) 14.
[22] E.M. Wewerka, E.D. Loughran, J.M. Williams, The Effect of Long-Term Storage at Elevated Temperature on Small Cylinders of PBX 9501, Los Alamos Scientific Laboratory Report: LA-6302-MS, Los Alamos, New Mexico 1976.
[23] J.S. Walker, J.B. Wills, J.P. Reid, L. Wang, D.O. Topping, J.R. Butler, Y.-H. Zhang, Direct Comparison of the Hygroscopic Properties of Ammonium Sulfate and Sodium Chloride Aerosol at Relative Humidities Approaching Saturation, J. Phys. Chem. A 114 (2010) 10.
[24] A.M. Giambra and C. J. Rosales, Determination of Molecular Weight and %Estane in Pressed PBX 9501 Samples by SEC/GPC (4, 6, 9, 12, 18, and 24 Months), Los Alamos National Laboratory, Internal lab. reports, Los Alamos, New Mexico, 2016-2020.
[25] G.W. Brown, A.M. Giambra, Examination of the Mw and Mp Data vs Columns, Los Alamos National Laboratory, Internal lab. report, Los Alamos, NM 87545, 2017, p. 13.
[26] S. Mori, H. Barth, Size Exclusion Chromatography, Springer, New York, 1999.
[27] Y.I. Mushkin, N.F. Smirnova, B.M. Tsigin, A.I. Finkel'shtein, IR and UV Spectra of Diaminodiphenylmethane isomers and the corresponding diisocyanates, Zhurnal Prikladnoi Spektroskopii 15(6) (1970) 5.
[28] H.H. Willard, L.L.J. Merritt., J.A. Dean, F.A.J. Settle, Instrumental Methods of Analysis, CBS Publishers & Distributor Pvt. Ltd., New Delhi, 1986.
[29] Shimadzu, Analysis of Polystyrene with Antioxidant Additive Using Prominence-i GPC System, 2021. https://www.shimadzu.eu/analysis-polystyrene-antioxidant-additive.
[30] N.S. Allen, Catalytic Thermal Oxidation of Phenolic Antioxidants by Hindered Piperidine Compounds, Polymer Degradation and Stability 3 (1980) 9.
[31] N.S. Allen, J.-L. Gardetie, J. Lemaire, Interaction between Antioxidants and Hindered Piperidines in the Photostabilisation of Propylene: Influence of Processing History, Polymer Photochemistry 1 (1981) 11.
[32] D. Yang, R. Pacheco, S. Edwards, K. Henderson, R. Wu, A. Labouriau, P. Stark, Thermal Stability of a Eutectic Mixture of Bis(2,2-dinitropropyl) acetal and formal: Part A. Degradation Mechanisms in Air and under Nitrogen Atmosphere, Polymer Degradation and Stability 129 (2016) 19.
[33] D. Yang, R. Pacheco, S. Edwards, J. Torres, K. Henderson, M. Sykora, P. Stark, S. Larson, Thermal Stability of a Eutectic Mixture of Bis(2,2-dinitropropyl) acetal and formal: Part B. Degradation Mechanisms under Water and High Humidity Environments, Polymer Degradation and Stability 130 (2016) 10.
[34] D. Yang, A. Edgar, J. Torres, J. Brett, C. Wong, FY2020 Progress Report of Aging and Lifetimes Program – Part II: Final Report of Four-Year Long Aging Experiment of Nitroplasticizer, Los Alamos National Laboratory, LA-CP-21-20217, Los Alamos, New Mexico, 2021, p. 31.

[35] X. Chen, M.E. Fuller, C.F. Goldsmith, Decomposition kinetics for HONO and HNO_2, Reaction Chemistry & Engineering 4 (2019) 11.
[36] R. Ballini, A. Palmieri, Nitroalkanes, Wiley-VCH, Weinheim, Germany, 2021.
[37] D. Yang, J. Jung, Impact of Nitroplasticizer (NP) Degradation on PBX 9501 Stability (Full Report), Los Alamos National Laboratory, LA-CP-21-20452, Los Alamos, New Mexico 2021, p. 96.
[38] D.A. Wrobleski, D.A. Langlois, E.B. Orler, J.R. Schoonover, J.H. Small, Thermal degradation studies of nitroplasticized estane® 5703 utilizing isotopic enrichment, Los Alamos National Laboratory, LA-UR-02-3428, Los Alamos, New Mexico, 2002.
[39] R.B. Rauch, R. Behrens, Vapor Pressures, Mass Spectra and Thermal Decomposition Processes of Bis(2,2-Dintropropyl)acetal (BDNPA) and Bis(2,2-Dinitropropyl)formal (BDNPF), Propellants, Explosives, Pyrotechnics 32(2) (2007) 20.
[40] H.H.G. Jellinek, T.J.Y. Wang, Reaction of Nitrogen Dioxide with Linear Polyurethane, Journal of Polymer Science 11 (1973) 16.
[41] P.W. Leonard, Mechanism of acetal (or formal) hydrolysis, Personal Communication, 2016, p. 2.
[42] D.K. Pauler, J.D. Kress, Nitroplasticizer Resistance to Hydrolysis, Personal Communication, 2006, p. 1.
[43] D. Yang, A.S. Edgar, J.A. Torres, J.C. O'Neel, C.H. Wong, FY2020 Annual Report of Aging and Lifetimes Program – Part II: Summary of Four-Year Long Aging Experiment of Nitroplasticizer, Los Alamos National Laboratory, LA-CP-21-20217, Los Alamos, New Mexico, 2021, p. 31.
[44] A.S. Edgar, C.H. Wong, D. Yang, Results of untargeted LC-QTOF analysis of eutectic bis(2,2-dinitropropyl) acetal/formal accelerated aging: implications on aging profiles, Los Alamos National Laboratory, LA-UR-22-20808, Los Alamos, New Mexico, 2022, p. 10.
[45] M. Soleimani, L. Dehabadi, L. D. Wilson and Lope G. Tabil, Antioxidants Classification and Applications in Lubricants, Chapter 2, IntechOpen, http://dx.doi.org/10.5772/intechopen.72621, 2018.
[46] B. Tao, G. Wang, Z. Yin, X. Pu, Y. Jiang, L. Zhang, J. Cheng, Y. Li, J. Zhang, Determination of the Contents of Antioxidants and Their Degradation Products in Sodium Chloride Injection for Blood Transfusion, Journal of Analytical Methods in Chemistry 2020 (2020).
[47] A. Edgar, J. Yang, M. Chavez, M. Yang, D. Yang, Physical Characterization of bis(2,2-dinitropropyl) acetal and bis(2,2-dinitropropyl) formal, J. of Energetic Materials (2020) 21.

Graphic abstract: Antioxidant (e.g., Irganox 1010) plays a critical role in scavenging oxidant/radical species occurring in plastic bonded explosive (PBX) 9501. As Irganox 1010 depletes, water and oxidants/radicals generated from nitroplasticizer (NP) degradation react with Estane through well anticipated hydrolysis, oxidation, and NP addition to change the properties of Estane over the aging process. Since more than one reaction can take place simultaneously, the molecular weight (MW) of Estane will change non-monotonically. The impacts of aging conditions on postulated degradation mechanisms of NP and Estane, and thus on changes in the MW of Estane are highlighted here when PBX 9501 is thermally aged under moderate temperatures.